Estimation of Rotor Position for Permanent Magnet Synchronous Motor at Standstill Using Sensorless Voltage Control Scheme

Fatih J. Anayi *, Mazen M. A. Al Ibraheemi

***Abstract*— The zero-speed rotor position estimation in surface mounted permanent magnet synchronous motor SM-PMSM represents a challenge due to the weak magnetic saliency in this type of motors. This paper presents a new method to estimate the initial rotor position of SM-PMSMs more simply and more accurately without any form of position or current sensors. It achieves this goal through an injection of three short width pulses and employing only the measurements of the motor terminal voltage responses, which fluctuate sinusoidally with the rotor position. Thereby, memory addresses, or dimensions of a look-up table, were created from the readings of the measured voltages. The memory was primarily loaded with 360 angles, each represents 1^o angle of rotor positions. The simulated MATLAB model and experimental results demonstrate the advantages. Comparing with the previous related publications, this research work has fulfilled two main contributions. The first is in achieving a rotor position estimation of 1^o resolution. The second is in eliminating the technique needed for detection of the rotor magnet polarity. The measured rates of error for the MATLAB model and the practical model were 2% and 5% respectively**

***Index Terms*— Magnetic saliency, SM-PMSM, rotor position estimation, voltages measurements, lookup table, dimensions of lookup table.**

I. Introduction

Over the past two decades, the permanent magnet synchronous motors, PMSMs, have become leaders among motor applications. The promising features of PMSM are summarized by its high efficiency, flexible control, robust operation, small size, identical high efficient relation among torque, power and speed, etc.[1]–[4]. These features are closely related to the accuracy of rotor position estimation. Moreover, starting-up the PMSM without accurate prior knowledge about the initial rotor position may cause a rotor stiffness or running in reverse direction. However, the reliance on sensors to realize this task involves significant drawbacks due to their high cost, unreliable usage and large size [5]–[7]. Many techniques have been presented to achieve sensorless rotor position estimation and running for PMSMs.

Most of the proposed methods are based on the detection of the inherent feature of rotor magnetic saliency. Therefore, the estimation of the rotor position at standstill and low speed in surface mounted permanent magnet synchronous motors SM-PMSMs is more difficult and complicated. It still represents a difficult challenge due to the very weak magnetic saliency in this type of motors [8]–[10]. Injection of a short width pulse in the stator windings and sensing the voltage and current responses at the motor terminals is adopted to obtain a low resolution rotor position estimation [11], [12]. Whereas, a technique of high frequency signal injection (HFSI) in the stator windings is also employed for zero and low speed rotor position estimation [13]. In both cases, there should be a technique to detect rotor magnet polarity. However, it is possible to apply a combination of both these methods to obtain the initial rotor position, where the HFSI estimates the primary position while the injection of short pulses indicates the polarity of the rotor magnet [8], [14]. In these approaches, apart from very large computational processes which are required and the complicated estimator circuitry, the estimation resolution still requires further improvement.

Other efforts for minimizing the drawbacks associated with the estimation of rotor position have been achieved. Reference [10] used the HFSI technique to study the effect of variations in the stator winding resistances on the accuracy of rotor position estimation. Whereas, [15] injected a HF voltage and estimated the rotor position from measuring the differences between the three current responses of the stator windings. Reference [16] confirmed that the accuracy of standstill SM-PMSMs rotor position estimation varies from one prototype of motor to another under the same test procedure. To address the very low L_q/L_d ratio in SM-PMSM, [17] proposed an approach based on establishing an overlap space between each pole and the corresponding stator tooth to create a zigzag linkage flux.

Demodulation method based on direct rather than synchronous signal injection, was proposed by reference [18] for initial rotor position estimation. This was to eliminate utilizing LPF in demodulation process which causes some limitations and drawbacks. In addition, it influenced the machine magnetic saturation to perform detection of magnetic polarity. It was concluded that the proposed method provides an accurate and reliable rotor position estimation. Although the key point of reference was to control SM-PMSM running at high speed with high inertial load, it was necessarily to tackle the standstill rotor position estimation. It was mentioned that no approach better than machine saliency for standstill rotor position estimation [19]. Reference [20] presented pulse

Fatih J. Anayi, Wolfson Centre for Magnetics, Cardiff University, Cardiff CF24 3AA, U.K, *Anayi@cardiff.ac.uk

Mazen M. A. Al Ibraheemi, Chemical Department, Faculty of Engineering, University of AL-Qadisiyah, Iraq, mazen.ali@qu.edu.iq

injection method to estimate the initial rotor position of doubly salient PM motors. It based on applying a series of pulsating signals on the stator windings. Then the voltage and current responses, which are supposed to carry information about the standstill rotor position, are analyzed. The results were shown that the proposed method either to estimate the position angle correctly or with a certain amount of average error rate of 1.4°. This method may suffer from rotor position shift during its estimation process if pulses of high amplitude or long duration are adopted.

The cited references can be classified, according to the method of estimation at standstill, into two categories; continuous carrier injection method and pulse injection method. The former can be extended to be applied on running speed close to zero speed. However, it suffers from complicated design, high cost and badly effect on the estimator bandwidth. Whereas the latter is of simple design and cost effective but it has a very low resolution of position estimation which is mostly sufficient for BLDC motor applications. Although the proposed approach, by this paper, well match the second method, it presents significant contributions by eliminating the polarity detection technique and providing an estimation of high resolution, 1°, by which it overrides the application on BLDC to PM motors.

This work addresses the difficulty of estimation the SM-PMSM rotor position through a new method. It fulfils a full sensorless rotor position estimation with high resolution through sensing the motor terminal voltage variations at different rotor positions. This can be achieved by creating two memory address lines which are employed to access a memory structure where the rotor angle positions are stored. These variations are exploited to create two dimensions which are employed to access a 2D-lookup table where the rotor position angles are stored in its cells. The proposed method has satisfied two significant novelties, an estimation of 1° resolution and an elimination of the magnet polarity technique. The paper has been organized into six sections as follows: the introduction which has been presented in section I. The theoretical background is reviewed in section II. Then section III introduces the work methodology. Section IV illustrates the MATLAB model. Section V describes the practical model and section VI summaries the conclusions.

II. THEORY

In permanent magnet motors, three magnetic fields associate within the motor magnetic circuit. They are; the stator fields (Φ_A, Φ_B and Φ_C), the permanent rotor field and the air gap field. As shown in Fig. 1, the magnetisation component of the permanent magnet field, d-component, linkages the stator windings. Depending on the rotor direction, this linkage field either enhances or weakens the stator winding field, i.e. magnetisation or demagnetisation effect. Therefore, the rotor magnet effect is sinusoidally oscillated between maximum and minimum limits. In a certain winding, e.g. winding A, a maximum magnetisation occurs when the d-axis of rotor field coincides the axial position of that winding. Vice versa, a maximum demagnetisation happens if the rotor magnetic direction and the stator field are in opposite directions. Topics of maximum magnetization and demagnetization are illustrated in Fig 1. The air gap has a contribution toward magnetisation and demagnetisation by affecting the influence of rotor field. In this work, the air gap impact is negligible as it has a weak and uniform distribution in SM-PMSMs.

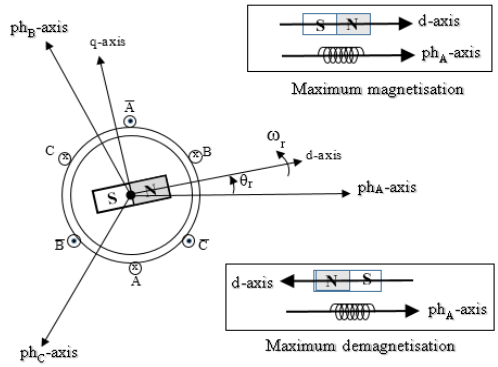

Fig. 1. Analytical view to the structure of PMSM and its magnetic fields and illustration for maximum magnetisation and demagnetisation

Consequently, as the numerator of the fundamental equation of a coil inductance ($L=\Delta\phi/\Delta i$) varies sinusoidally, the corresponding stator winding inductances also have a sinusoidal variation with rotor position. This will lead to a similar variation at rotor terminal voltages, which could be exploited in prediction of the standstill magnet position. So, the measured terminal voltages could be used to create two address lines, x and y. Creation of x and y dimensions will be illustrated in detail in the next section. The dimensions are employed as address lines to access a memory structure whose contents are the all-possible rotor angular positions. Figure (2) shows an overall view for this concept.

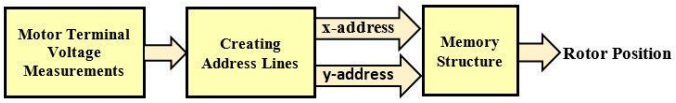

Fig. 2. The proposed concept for rotor position estimation at standstill

Testing of PMSMs could be based on the excitation of only two of stator windings at any moment of time, while the third stator winding could be employed as a sensor to measure the terminal voltages [21], [22]. This concept was applied in this work by injecting a short duration pulse into any two of the three motor windings, which form a two-inductor series loop. The third unexcited winding was used as a sensor to measure the voltage drops on the excited winding terminals. Figure (3a) illustrates the application of a short pulse of duration width (150μs) at the gates of the switching elements (IGBTs) which respond by switching to the ON condition. The responses of the IGBTs produce a voltage pulse between the terminals of motor windings A and B. The amplitude of this pulse equals the dc link voltage V_{dc} and its duration equals that of the applied pulse on the gate of the switching element.

Then, the measured voltage between the free terminal of winding C and the ground indicates the value of voltage drop

between the neutral point N and the other terminal of coil B. So, this voltage is labelled V_{NB1} where the subscript '1' refers to the measured voltage at motor terminal C due to the first pulse. After 150μs has elapsed, the switching element takes the OFF condition and the connection of coil terminals A and B is reversed via the freewheel diode. At this moment, the free terminal of winding C senses the voltage drop in winding A during the freewheeling period which is labelled as V_{NAF1}, where the subscript 'F1' refers to the freewheeling period caused by the absence of the first pulse. The same events are repeated when the second and third pulses fire the IGBTs to yield the motor terminal voltages V_{NC2}, V_{NAF2}, V_{NC3} and V_{NBF3}. These are illustrated in Figs. (3b) and (3c).

As a result, six voltage measurements are obtained at the motor terminals during the active and passive periods of the three pulses, V_{NB1}, V_{NAF1}, V_{NC2}, V_{NAF2}, V_{NC3} and V_{NBF3}. These voltages are employed to create two dimensions, or addresses, x-dimension and y-dimension which are used to access the cells of the 2D-lookup table, or memory structure, where the angles of rotor positions are stored.

III. METHODOLGY OF FORMATTING THE MEMORY ADDRESS LINES

As aforementioned, six terminal voltages could be extracted as impulse responses for injection of three pulses into the motor stator windings. Comparing these voltages with each other could be utilized to create the x-dimension. Meanwhile, voltage variations of one of the responses could be employed in formatting the y-dimension.

A- Formatting the x-dimension

The results obtained from modelling the undertaken SM-PMSM, which has three pole pairs, reflect that the total rotor spatial is divided into six sectors (S_1 to S_6). Each sector is further divided into six subsectors, (S_{11} to S_{16}) for sector1 and (S_{21} to S_{26}) for sector2 and so on, where each of the sub-sectors covers angle of ten degrees. This sectors division is clearly illustrated in Table I. The subscripts "n" and "m" vary from 1 to 6 to indicate the sector or sub-sector numbers respectively. Consequently, the rotor space of a three pole-pairs is divided into 36 sub-sectors each of ten degrees angle.

As it is shown in Table I the first sub-sector, in main sector1, starts at rotor position "0^0" and ends at rotor position "9^0". Then it proceeds by adding an angular space of value 60(m-1), where "m" represents the sub-sector number. Therefore, the second sub-sector extends between "60^0" and "69^0" of rotor positions, and so on. Same manner is applied for the rotor positions of the rest of sub-sectors in the main sectors 2 through 6, regarding the angle of start position for each sub-sector.

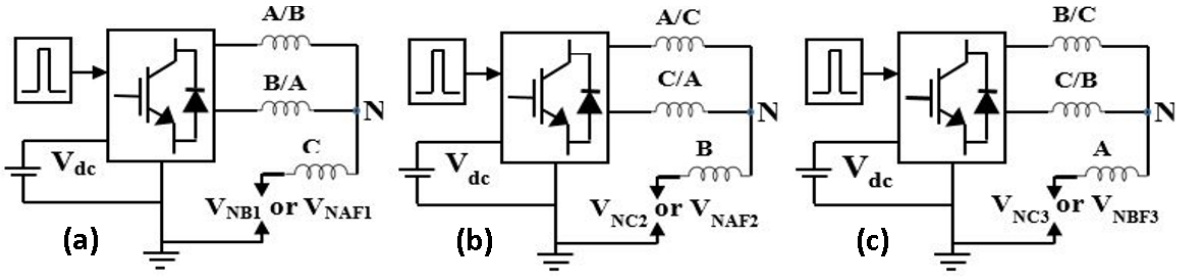

Fig. 3. Winding excitations by the three pulses

TABLE I
DISTRIBUTION OF ROTOR POSITION ANGLES INTO MAIN AND SUB-SECTORS S_{NM}

S_{nm}		Sector No. (n)					
		1	2	3	4	5	6
Sub-sector No. (m)	1	0° to 9°	10° to 19°	20° to 29°	30° to 39°	40° to 49°	50° to 59°
	2	60° to 69°	70° to 79°	80° to 89°	90° to 99°	100° to 109°	110° to 119°
	3	120° to 129°	130° to 139°	140° to 149°	150° to 159°	160° to 169°	170° to 179°
	4	180° to 189°	190° to 199°	200° to 209°	210° to 219°	220° to 229°	230° to 239°
	5	240° to 249°	250° to 259°	260° to 269°	270° to 279°	280° to 289°	290° to 299°
	6	300° to 309°	310° to 319°	320° to 329°	330° to 339°	340° to 349°	350° to 359°

Figure (4) shows a block diagram for the hardware view to detect the main sectors within the rotor spatial of the motor under test. Detection of the main sectors depends on fifteen comparisons between the six measured voltages at the motor terminals aforementioned in section II, V_{NB1}, V_{NAF1}, V_{NC2}, V_{NAF2}, V_{NC3} and V_{NBF3}. In this work, the fifteen comparisons were denoted by logic variables x_1 through x_{15}. Comparing the first measured voltage with the other five voltages gives the logic values, 0 or 1, of x_1 through x_5 respectively. Comparisons of the second measured voltage with the other four voltages determine the logic values of x_6 through x_9 respectively. Similarly, the logic values of x_{10} to x_{15} are obtained. The following formula is used to format x-address.

$$\text{x-address} = x_1+2x_2+3x_3+ \ldots. +15x_{15} \quad (1)$$

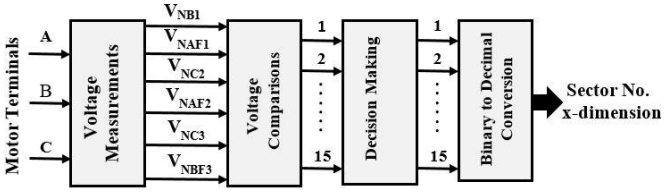

Fig. 4: Formatting the x-dimension

B-Formatting the y-dimension

The mathematical model of SM-PMSM at standstill is given by the following equation: [16]

$$\begin{bmatrix} V_A \\ V_B \\ V_C \end{bmatrix} = \begin{bmatrix} R_A & 0 & 0 \\ 0 & R_B & 0 \\ 0 & 0 & R_C \end{bmatrix} \begin{bmatrix} I_A \\ I_B \\ I_C \end{bmatrix} + \begin{bmatrix} L_A & -M_{AB} & -M_{AC} \\ -M_{BA} & L_B & -M_B \\ -M_{CA} & -M_{CB} & L_C \end{bmatrix} \frac{d}{dt} \begin{bmatrix} I_A \\ I_B \\ I_C \end{bmatrix} \quad (2)$$

With each pulse injection, two of the three stator windings combine in a series loop, with a common excitation current, to form one coil. So, there is no active mutual between them. While the third winding is non-excited, so it is non-active (Fig. 3). Thereby, there are no mutual inductances between the three windings. So, eq.(2) for the undertaken PMSM model could be expressed by the following equation where the mutual inductances are omitted:

$$\begin{bmatrix} V_{NB1} \\ V_{NC2} \\ V_{NC3} \end{bmatrix} = \begin{bmatrix} R_A + R_B & 0 & 0 \\ 0 & R_A + R_C & 0 \\ 0 & 0 & R_B + R_C \end{bmatrix} \begin{bmatrix} I_{AB} \\ I_{AC} \\ I_{BC} \end{bmatrix} + \begin{bmatrix} L_A & 0 & 0 \\ 0 & L_B & 0 \\ 0 & 0 & L_C \end{bmatrix} \frac{d}{dt} \begin{bmatrix} I_{AB} \\ I_{AC} \\ I_{BC} \end{bmatrix} \quad (3)$$

Individually, if the voltage V_{NB1} is considered as an example for voltage analysis, then, referring to Fig. (3a) and eq.(3), it could be written as follow:

$$V_{NB1} = V_{dc} \frac{Z_B}{Z_A + Z_B} \quad (4)$$

where Z_A and Z_B are the impedances of windings A and B respectively and V_{dc} is the dc link voltage.

In complex form, eq.(4) can be re-written as:

$$V_{NB1} = V_{dc} \frac{R_B + j\omega L_B}{(R_A + R_B) + j\omega(L_A + L_B)} \quad (5)$$

where L_A and L_B are the inductances of windings A and B respectively, which under the influence of magnetic saliency, are expressed as:

$$L_A = L_{av} + \Delta L \cos(\theta), \; L_B = L_{av} + \Delta L \cos\left(\theta - \frac{2\pi}{3}\right) \quad (6)$$

L_{av} is the nominal value of the phase inductance and ΔL is the maximum variation in inductance value due to the effect of magnetic saliency. As 'ω' in eq. (5) is an angular frequency and it is equivalent to the switching speed of the IGBTs which is normally of a very high value, hence, the resistive components in both numerator and denominator of eq.(5) could be omitted compared to the correspondingly high inductive components. Therefore, eq.(5) could be re-written as:

$$V_{NB1} = V_{dc} \frac{L_B}{L_A + L_B} \quad (7)$$

Eq. (7) expresses the measured voltage V_{NB1} as a function of the values of winding inductances L_A and L_B. As these inductances are functions of rotor position affected by the rotor magnet saliency, so, indirectly, the measured voltage will be a function of rotor position as well. Consequently, the voltage V_{NB1} will fluctuate highly as there is a remarkable increase in the machine saliency within the rotor spatial space.

This deduction is supported and clearly noticeable in Fig. (5), where the measured voltage V_{NB1} at the terminals of surface mounted and interior PMSMs are given. The figure was plotted by exporting the data of the measured voltage, V_{NB1}, from the MATLAB workspace to Microsoft excel. It is clear that V_{NB1} has a remarkable fluctuation with variation of rotor position in the interior type PMSM, 200V peak to peak fluctuation versus 0.6V for the surface mounted type. This result reflects the considerable weakness of the saliency in SM-PMSM and how it affects the voltage responses.

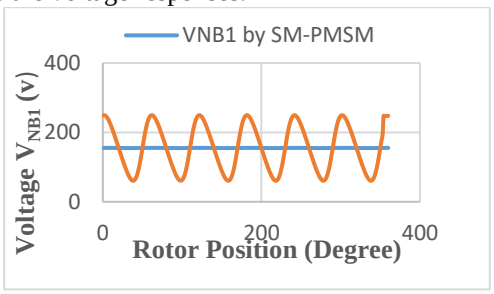

(a)

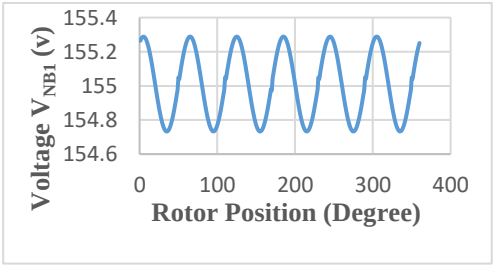

(b)

Fig. 5: Voltage VNB1 oscillation due to rotor saliency in; (a) IPMSM and SM-PMSM, (b) SM-PMSM only

This saliency makes the inductances in (7) slightly variable with rotor position. Accordingly, the measured voltage V_{NB1} is of a marginal variation with rotor angle. Currently, literatures have not presented any solution for SM-PMSM rotor position sensing other than exploiting that marginal saliency effect. Thereby, this technique took advantage of the weak variation at motor terminals to format the second dimension of the 2D-lookup table. Figure (6) illustrates a practical view for the method of formatting this dimension. After measuring the terminal voltage, V_{NB1} in Fig. 6, it should be modified by removing the dc component and being amplified, according to a certain algorithm, to maximize the differences among the measured voltages at different rotor positions.

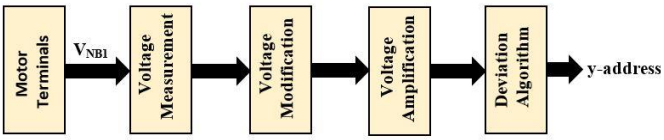

Fig. 6: Formatting the y-dimension

. It may be worth to mention that any of the measured voltages is the potential difference between the free terminal of the non-excited machine winding and the common terminal of the dc bus voltage. So, there is no need to access the stator windings neutral point.

IV. MODEL STRUCTURE AND SIMULATION RESULTS

A- Model structure

The simulated system for standstill SM-PMSM rotor position estimation is given in Fig. (7). All the figure blocks were picked up from, or built using, the "Simulink library". The pulse generator and inverter block generate the injection pulses and injects them into the motor windings via an inverter. Each motor terminal voltage is of two different periods, forward and flywheel. Voltage measurements are performed, by voltmeter model, nearly at half of each period to avoid the oscillations at the period edges. So, the voltage measurements block provided six voltages which are compared to produce the x-dimension utilizing eq. (1). Whereas, the y-dimension is established from the millivolt variations in one of the six measured voltages. In this work V_{NB3} was arbitrarily chosen to achieve this issue after passing through the modification and amplification block. Cells of the 2D-lookup table are pre-loaded by all rotor position angles to output the position estimation when addressed by x and y dimensions.

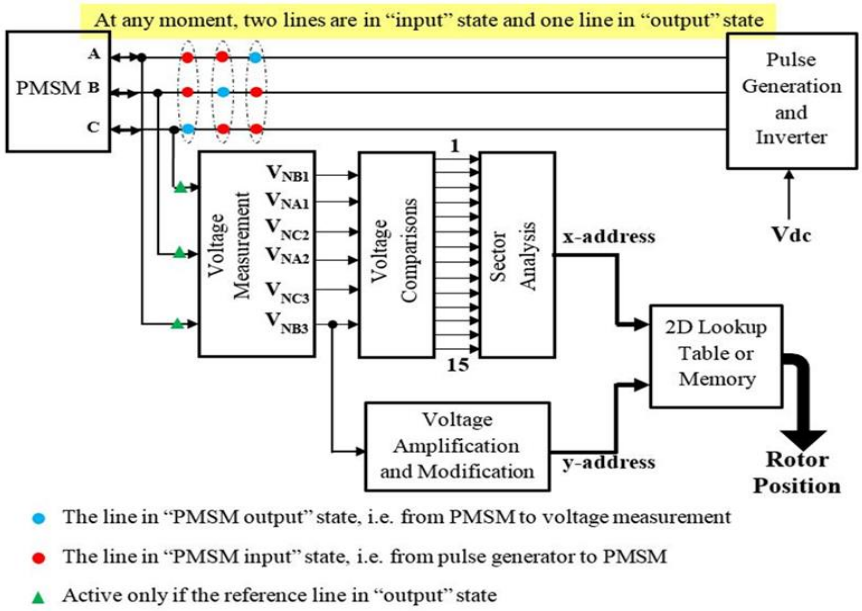

Fig. 7: MATLAB implementation for the proposed rotor position estimator at zero speed

B- Simulation results

The proposed estimator provided 360 estimated rotor positions, each of which corresponds to an actual rotor position. As pole-pairs of the simulated motor was three, the whole spatial of the rotor was divided equally among six main sectors, and the space of each main sector was further divided over six sub-sectors. Figure (8) illustrates this division for a rotor of three pole-pairs.

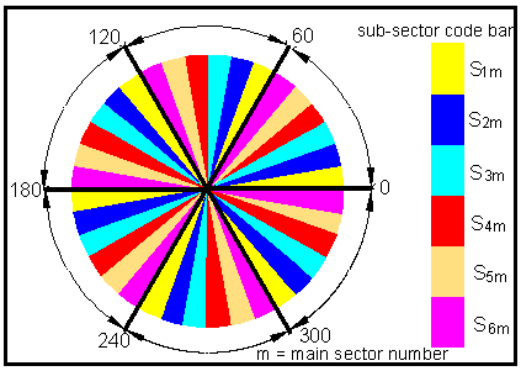

Fig. 8: Main sectors and sub-sectors division for a rotor of three pole-pairs

The rotor positions in the main and sub-sectors were pointed out by the formatted x and y dimensions. It is found that the proposed estimator has a 2% failure rate and the y-dimension is the source of this failure because some values of the y-dimension were too close to each other to be distinguished by the model. This is because they are derived originally from a voltage of winding which is under the influence of weak saliency. To tackle this obstacle, an exponential function algorithm is adopted to maximize the differences among the values of y-dimension and thereby an efficient addressing is obtained. Key topic of this algorithm is taken from the equation of diode current in forward direction when a little change in diode voltage causes a big change in diode current. So, the y-dimension value is put as the power index of the exponential function. Then, the resultant algorithm value is used as the new y-dimension value [23].

Figure (9) is a two-dimension plane which is intended hereby to highlight this point at main sector 1. This sector has divided into six sub-sectors, distributed over the angles 0^0-9^0, 60^0-69^0, and so on as shown in figure (8). Considering the presence of six sub-sectors within each main sector, each rotor position on the horizontal axis is actually assigned for other five positions by adding 60(m-1) to the numbers on the horizontal axis, where m is the main sector number. For instance, number "1" on the horizontal axis may refer to rotor positions "1", "61", "121", "181", "241" or "301" as m is an integer varies from 1 to 6. The corresponding y-dimension, y-address, values are projected on the two-dimension coordinate plane and those of contiguous points are circled. These points are hard to be discriminated because they have the same x-address and very closed y-address values. So, they need more manipulation to be distinguishable by the proposed model.

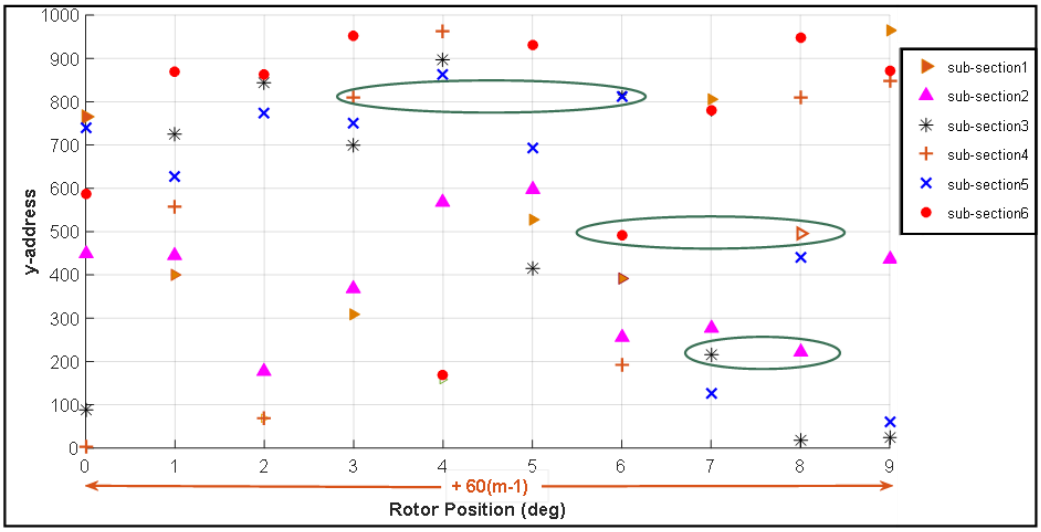

Fig. 9: The values of y-dimension line at main sector1

The simulated estimation model was tested on a motor whose specifications are listed in Table II (M-0200) but with 310V dc link voltage. The obtained results for the simulated estimator model of standstill rotor position are combined with the practical results and to be explored later in figure (12). Each of the apparent peaks in the figure represents a failure where a dual position estimation corresponding to a certain actual rotor position has been occurred.

V. PRACTICAL MODEL

A- Description and principle of operation

The experimental works on a practical model were carried out using two SM-PMSMs types "M-0200-104-4-000" and "ACM-2n320-4/2-3" at standstill and under room temperature. The details of the motors' specifications are given in Table II. An 8-bit microcontroller type "AVR ATmega2560" was employed to generate 5V, 3kHz injection pulses and to perform the calculations for the standstill rotor position estimation. The inverter was supplied with 24V direct voltage and fired by the injected pulses.

Furthermore, the voltage responses at the motor terminals were sensed through exploiting the analogue input terminals of the employed microcontroller. Whereas, the embedded microcontroller analogue to digital converter, 10-bit ADC, worked as voltage sensors and permitted to measure the voltage responses with less than 5mV resolution. The look-up table in the MATLAB model was implemented in the practical model by some form of EEPROM, whereas the x and y dimensions were combined to form the memory address. To meet the research goal, which represented by the zero-speed rotor position estimation, all the tests were done at room temperature as the motor is at standstill. Therefore, there was no discussion about the motor running condition or rotor temperature rising due to motor running.

An arbitrary light load was applied to the rotor shaft just to damp the rotor response to the injected pulses, where the repeating injection of pulses lead to accumulated rotor position shifts which formed finally a noticeable rotor position difference from the initial standstill setting.

TABLE II
SPECIFICATIONS OF MOTORS UNDER TEST USED IN PRACTICAL MODEL

Parameter	Value	
	M0200-104-4-000	ACM2n320-4/2-3
No. of phases	3	3
No. of poles	6	6
Stator Phase Resistance	0.6 Ohms	1 Ohms
Stator Phase Inductance	1.7mH	4.2mH
emf constant	11 (V/1000.min^{-1})	30 (V/1000.min^{-1})
Inertia	0.000018(kg.m^2)	0.00042(kg.m^2)
Rated Speed	3000 rpm	4000 rpm
Rated Power	200W	1.34kW
DC Link Voltage	48V	320V

Figure (10) is a schematic diagram to illustrate details of the practical model. The measured voltage responses had dc offset values, which made the responses of values greater than the voltage specification of the controller. Therefore, a subtracted voltage was necessary to remove these offset voltages to make the motor terminal voltages compatible with the microcontroller specifications.

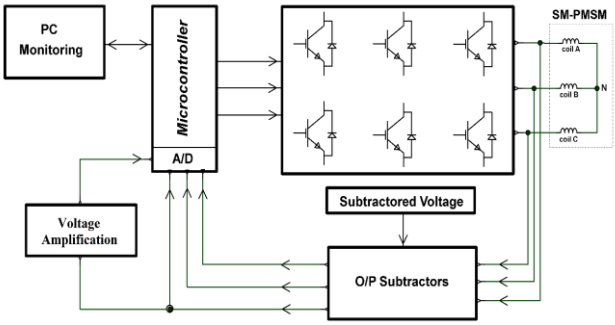

Fig. 10: Schematic diagram for the practical model

Figures (11a) shows the various parts that were used in implementation of the practical platform. Figure (11b) demonstrates a scope vision for the three injected pulses and the three corresponding voltage responses at motor terminals when the rotor of motor M-0200-400 at position 30^0.

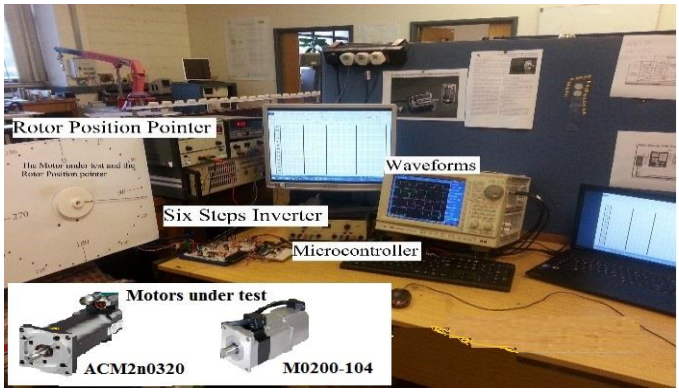

(a)

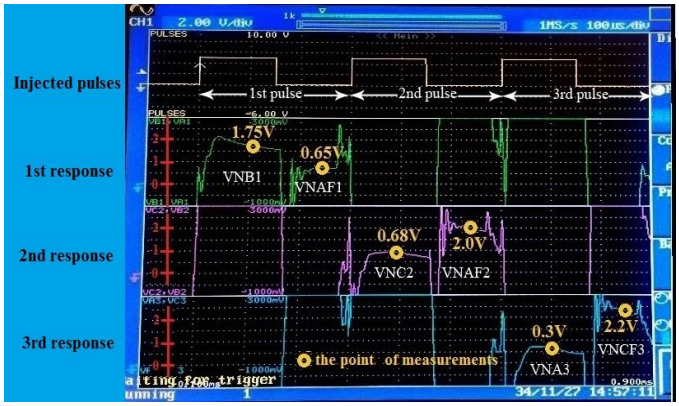

(b)

Fig. 11: (a) Practical platform (b) Experimental, three voltage responses at rotor position 30^0

Detailed explanation for figure (11b) is given below:

- Four plots are given, the first is for the three injected signals, while the second, third and fourth plots are for the voltages, which are measured at the motor terminals of windings C, A and B respectively.
- Let us consider the second plot during the period of first pulse, the terminal of winding C will be free, as illustrated in Fig (3a), and it could be used to monitor the terminal voltages of windings B and A during the high level and low level periods of the 1st pulse, so the microcontroller is ordered to measure the voltage V_{NB1} and V_{NAF1} respectively.
- The microcontroller was programmed to take the voltage readings exactly at the points, which are indicated by yellow circles. This is to avoid the oscillations, which appears at the waveform edges. Meanwhile, the snubber hardware structure at the switching elements terminals has an efficient contribution in suppressing any form of noise or oscillations due to high switching frequency of injected signals.
- The microcontroller compares these voltage readings to extract the sector number from which the x-address is extracted.
- The millivolt variations in the measured value of the voltage V_{NB1} with rotor position is taken as a base to create the y-address.

Measurement procedure, according to above points, was repeated 360 times for the simulated and practical models. Hence, 360 rotor position estimations were obtained for each model. The obtained results of rotor position estimation by both models are given in Fig. (12), where the measured via actual rotor positions are plotted. The correct estimation points are aligned in a straight line, whereas the peaks represent errored estimations. For instance, in Fig. (12b), when the rotor is at actual position 40^0, the proposed practical estimator estimates it wrongly by the peak e_2 which represents an estimated rotor position of 130^0.

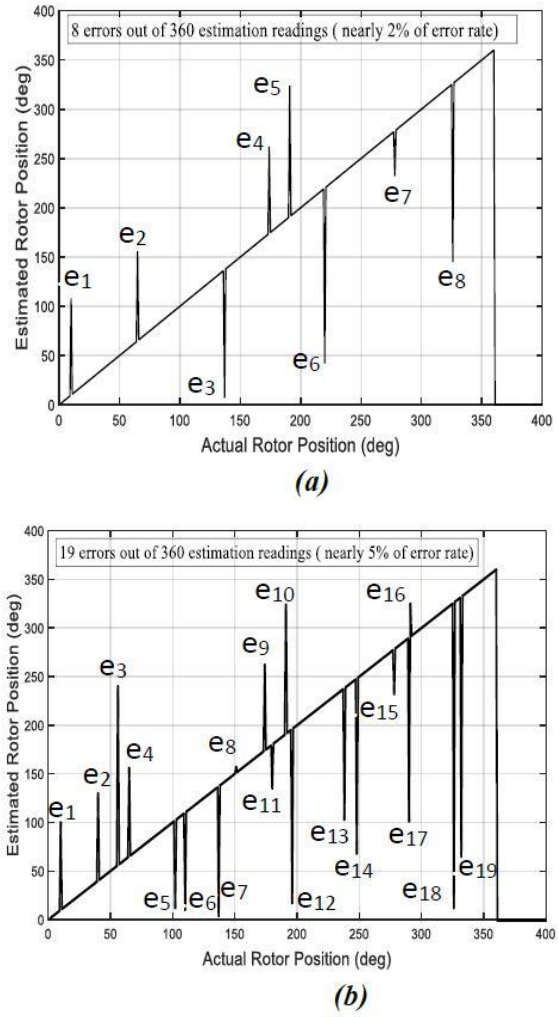

Fig. 12: Rotor position estimation (a) MATLAB model (b) practical model

Thereby, the proposed estimator introduces either correct or wrong estimation for the rotor position angle. There is no error margin for each angle estimation. Table III summarises the error estimations via the actual positions. Then the error rate has been calculated as the percentage ratio of the total error estimations, 19, to the total number of rotor position estimations, 360.

TABLE III
ERROR IN ROTOR POSITION ESTIMATIONS AGAINST THE ACTUAL POSITIONS

Actual	Estimated	Error	Actual	Estimated	Error
14	100	e_1	191	324	e_{11}
40	130	e_2	195	9	e_{12}
56	240	e_3	238	103	e_{13}
65	156	e_4	248	168	e_{14}
100	10	e_5	378	232	e_{15}
110	6	e_6	290	101	e_{16}
137	4	e_7	291	325	e_{17}
151	157	e_8	326	12	e_{18}
174	262	e_9	332	65	e_{19}
180	135	e_{10}	---	---	---

The absolute errors are obtained as the difference between the estimated and actual positions and are given by Fig. (13).

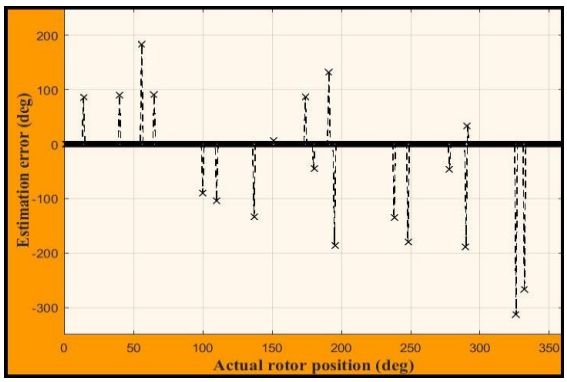

Fig. 13: Absolute estimation errors as the difference between estimated and actual positions versus the actual rotor position

Figure (14) is a flowchart for the process of estimation by the practical proposed method.

B- Comparison of MATLAB and practical models Results

Comparison between the MATLAB and practical model results indicates that there are two main sources for estimation error. The first is the rotor magnet symmetry which affected both models, and the second represents the noise which is clearly noticed in the practical responses. This noise random oscillation emerges as a resulted of multiple magnetic saliencies, the saturation effect and the high-speed switching's ON and OFF of electronic components, IGBTs, of the practical model. The effect of the former appeared on both models, practical and MATLAB, whereas the latter impact was noticed on the practical model only because the MATLAB calculations are based on a set of differential equations algorithm so they are immunised against the effects of the second source of error. This is the reason for the lower rate of error for the MATLAB model; 2%, compared with that for the practical model of 5%. For the same reason, the MATLAB consistent distributions of the rotor sectors and sub-sectors, given in Table I, were not

evident in practical model. However, the practical model employed this inconsistency to reduce the problem of rotor magnet polarity.

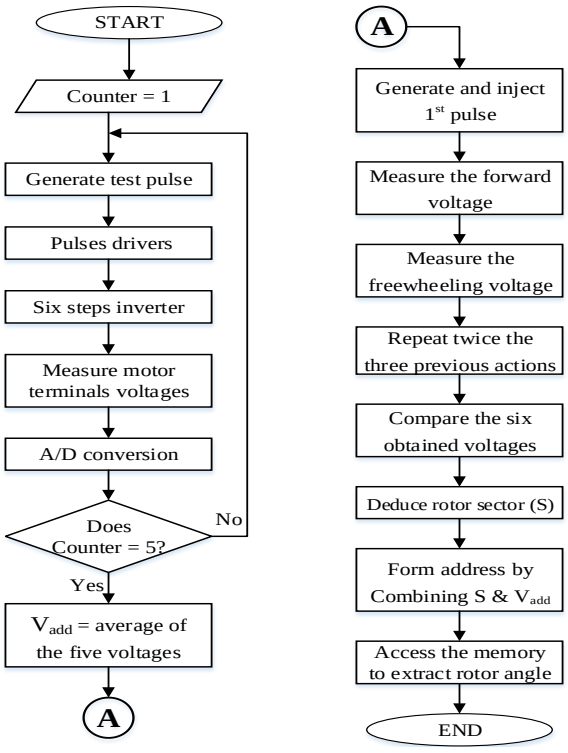

Fig. 14: Flowchart for position measurements

C-Comparison with other related works

Comparing with other related techniques, the proposed method is characterised by its simplicity, fast estimation and high reliability. The dispensing of magnetic polarity and adopting only the voltage measurements are the major contribution in the simplicity of the presented technique. The exclusive voltage measurements reduce the complexity of current measurements and making the model full sensorless through excluding the currents sensors. No large computing processes are required so that the estimated results are obtained within a short time, i.e. a few hundreds of microseconds. The 1^o resolution for rotor position estimation provides a clear and promising difference between this proposed approach and the other relevant mechanisms. Table IV shows a comparison summary for the results of the proposed method and other relevant works as given by the references [11], [16], [20], [24]–[26]. The large difference between the obtained resolution by the proposed method and the other references, except reference [20], is because the other references were working on BDCM but not on PMSM, where this resolution is acceptable to run such motors. So, they only regarded the comparison results, x-dimension.

TABLE IV
COMPARING THE RESULTS OF THE PROPOSED METHOD WITH THE PREVIOUS RELATED WORKS

	Ref 11	Ref 16	Ref 20	Ref 24	Ref 25	Ref 26	proposed
Resolution (degrees)	30	Not given	1	22.5	60	60	1
Magnet polarity	Yes	Yes	Yes	Yes	Yes	NO	No
Current sensors	1/dc-link current	1/dc-link current	3/phase current	3/phase current	1/dc-link current	1/dc-link current	No
Voltage certainty	good	good	good	good	good	good	Weak
Error rate	Not given	7.64^o	Varies with rotor position	Varies with rotor position	Not given	Not given	5%

VI. CONCLUSIONS

A novel method, of error rate around 5%, has been presented in this paper to estimate the rotor standstill position of SM-PMSM. It can be concluded that the novelty has been validated by three promising achieved improvements which may maintain immune motor start up. Firstly, it exploits only the motor voltages terminals to obtain measurable voltage differences for each rotor position, so no current measurements, and current sensors, were required. Secondly, eliminating the detection of magnet polarity led to simplify the structure of the proposed angle-sensorless rotor position estimator. Finally, the achievement of 1^0 resolution for rotor position estimation represented a significant progress comparing with other techniques. This resolution is sufficient to maintain soft and robust motor running, but it could be improved via adopting electronic devices of higher capability in measuring and analysis the motor voltage responses. It is also deduced that the number of main sectors, which divides the rotor spatial, is equal to the number of poles that are mounted on the rotor surface, whereas the sub-sectors distribute according to the space of the main sector. This proposed method may encounter some limitations which represented by the challenge of maintaining stable voltage readings. Although the voltage variations have less effect on specifying the sector number, and so the sector portion in address formatting (x-address), their effect is noticeable on voltage portion (y-address formatting). So, a robust measuring for this voltage is necessary to obtain accurate estimation of the rotor position. Increasing the resolution of the ADC could improve the voltage measurement accuracy and significantly reduce the rate of error. The proposed method could be applied more efficiently on other

motor types, such as IPMSM, because the SM-PMSM has the worst saliency and voltage responses. This work may have a lot of reference values through eliminating any hardware of position sensors and magnet polarity techniques. Therefore, it could inspire more future researches to strengthen this approach

REFERENCES

[1] P. Dost, "Mechanical and Electrical Behaviour of an Electric Vehicles Drive Train due to the Choice of the Control-System," *IECON 2011 - 37th Annu. Conf. IEEE Ind. Electron. Soc.*, pp. 1426–1431, 2011.

[2] M. Comanescu and I. Member, "Speed and Rotor Position Estimation of the PMSM by SM Observers with Compound Manifolds and Linear Feedback," *9th Int. Conf. Compat. Power Electron.*, pp. 317–322, 2015.

[3] A. K. Jebai *et al.*, "Sensorless position estimation and control of permanent-magnet synchronous motors using a saturation model," *Int. J. Control*, vol. 7179, no. February, 2016.

[4] G. Wang, R. Yang, Y. Wang, Y. Yu, and D. Xu, "Initial Rotor Position Estimation for Sensorless Interior PMSM with Signal Injection," *Int. Power Electron. Conf. - ECCE ASIA*, pp. 2748–2752, 2010.

[5] H. Sira-ramirez, "On the sensorless rotor position control of the Permanent Magnet Synchronous Motor : An Active Disturbance Rejection Approach," *13th Int. Conf. Power Electron.*, pp. 12–17, 2016.

[6] R. S. A and S. Wekhande, "Comparison of High Frequency Signal Injection Techniques for Rotor Position Estimation at Low Speed to Standstill of PMSM," *5th India Int. Conf. Power Electron.*, 2012.

[7] G. Meng, H. Yu, M. Hu, and L. Huang, "Initial Position Estimation of Permanent Magnet Synchronous Motors Based on Variation Behavior of Winding Inductances," *9th Int. Conf. Power Electron. ECCE Asia (ICPE-ECCE Asia)*, pp. 1609–1616, 2015.

[8] S. Yang, "Saliency-Based Position Estimation of Permanent-Magnet Synchronous Machines Using Square-Wave Voltage Injection With a Single Current Sensor," *IEEE Trans. Ind. Appl.*, vol. 51, no. 2, pp. 1561–1571, 2015.

[9] H. Zhaobin, Y. Linru, and W. Zhaodong, "Sensorless initial rotor position identification for non-salient permanent magnet synchronous motors based on dynamic reluctance difference," *IET Power Electron.*, vol. 7, no. January, pp. 2336–2346, 2014.

[10] M. Ali, G. Moghadam, and F. Tahami, "Sensorless Control of PMSMs With Tolerance for Delays and Stator Resistance Uncertainties," *IEEE Trans. POWER Electron.*, vol. 28, no. 3, pp. 1391–1399, 2013.

[11] N. S. Pillai and R. Radhakrishnan, "Analysis And Simulation Studies For Position Sensorless BLDC Motor Drive With Initial Rotor Position Estimation," *Int. Conf. Nascent Technol. Eng. F.*, 2015.

[12] B. Liu, B. Zhou, J. Wei, H. Liu, J. Li, and L. Wang, "A rotor initial position estimation method for sensorless control of SPMSM," *40th Annu. Conf. IEEE Ind. Electron. USA*, pp. 354–359, 2014.

[13] H. Kim, K. Huh, R. D. Lorenz, and T. M. Jahns, "A Novel Method for Initial Rotor Position Estimation for IPM Synchronous Machine Drives," pp. 1173–1180, 2003.

[14] G. Wang, R. Yang, W. Chen, Y. Yu, D. Xu, and C. C. Chan, "Initial Position Estimation for Sensorless Surface- Mounted PMSM with Near-Zero Saliency at Standstill," *IEEE Veh. Power Propuls. Conf.*, pp. 1403–1406, 2009.

[15] D. Wang, C. Zhou, M. Zou, J. Liao, and Y. Du, "Study on Inspection of the Initial Rotor Position of BLDC Based on High-frequency Signal Injection," *IEEE Conf. Expo Transp. Electrif. Asia-Pacific (ITEC Asia-Pacific)*, pp. 1–4, 2014.

[16] H. A. Toliyat and X. Wang, "Standstill Position Estimation of SPMSM," *38th Annu. Conf. IEEE Ind. Electron. Soc.*, pp. 2024–2029, 2012.

[17] S. Yang, R. D. Lorenz, and T. M. Jahns, "Surface Permanent Magnet Synchronous Machine Design for Saliency-Tracking Self- Sensing Position Estimation at Zero and Low Speeds," *IEEE Trans. Ind. Appl.*, pp. 3493–3500, 2010.

[18] X. Zhang, H. Li, S. Yang, and M. Ma, "Improved Initial Rotor Position Estimation for PMSM Drives Based on HF Pulsating Voltage Signal Injection," *IEEE Trans. Ind. Electron.*, vol. 65, no. 6, pp. 4702–4713, 2018.

[19] Q. Li, X. Wang, J. Jiang, Q. Zhang, and Q. Tong, "Sensorless Control for Surface Mounted PM Machine with a High Inertial Load," *Trans. Electr. Mach. Syst.*, vol. 2, no. 1, pp. 116–122, 2018.

[20] S. Li, S. Zheng, X. Zhou, and J. Fang, "A Novel Initial Rotor Position Estimation Method at Standstill for Doubly Salient Permanent Magnet Motor," *IEEE Trans. Ind. Informatics*, vol. 14, no. 7, pp. 2914–2924, 2018.

[21] Z. Chen *et al.*, "Sensorless Control for SPMSM With Concentrated Windings Using Multisignal Injection Method," *IEEE Trans. Ind. Electron.*, vol. 61, no. 12, pp. 6624–6634, 2014.

[22] K. Iizuka, H. Uzuhashi, M. Kano, T. Endo, and K. Mohri, "Microcomputer Control for Sensorless Brushless Motor," *IEEE Trans. Ind. Appl.*, vol. I, no. 4, pp. 595–601, 1985.

[23] D. W. Jordan and and P. Smith, *Introduction for the Engineering, Physical, and Mathematical Sciences*, 3rd ed. New York: Oxford University Press.

[24] P. B. Schmidt, M. L. Gasperi, and A. H. Wijenayake, "Initial Rotor Angle Detection of a Non-Salient Pole Permanent Magnet Synchronous Machine," vol. 00, no. c, pp. 8–12, 1997.

[25] G. H. Jang, J. H. Park, and J. H. Chang, "Position detection and start-up algorithm of a rotor in a sensorless BLDC motor utilising inductance variation," *IEE Proc. - Electr. Power Appl.*, vol. 149, no. 2, p. 137, 2002.

[26] Y. Lai, S. Member, F. Shyu, and S. Tseng, "New Initial Position Detection Technique for Three-phase Brushless DC Motor without Position and Current

Sensors," *IEEE Trans. Ind. Appl.*, pp. 1653–1660, 2002.

Fatih Anayi was born in Baghdad. He received a BSc degree in Electrical and Electronic Engineering from University of Baghdad in 1975 and following this, he worked with industry in Iraq for ten years. He received his MSc and PhD degrees from University of Wales/Cardiff in 1988 and 1992 respectively. He is working at Cardiff University/School of Engineering since 1992 as a researcher and academic, lecturing advanced power electronics and electrical machines & drives for under-graduate students in addition to supervising MSc and PhD students. He has published over sixty journal and conference papers related to electrical machine design, electromagnetic and power electronics. He participated in writing of two books, "Analogue Electronic Circuits and Systems" from Cambridge University Press, in 1991 and the second book was "Permanent-Magnet DC Linear Motors" from the Oxford University Press, 1996.

Mazen Al Ibraheemi was born in Najaf-Iraq. He received a BSc degree in Electrical and Electronic Engineering from University of Basrah in 1983 and following this, he has worked in higher education in Iraq up to now. He received his MSc degree from University of Technology/Iraq in 1994 and PhD degree degrees from Cardiff University/School of Engineering in 2018. Currently, he is working at faculty of Engineering/ University of Al Qadisiya as a researcher and academic lecturing in different electrical and electronics subject for under-graduate students. He has published over ten journal and conference papers related to electrical machine design, electromagnetic and electronics. In addition, he has many works as a consultant for electrical works and design in Scientific and Engineering Services bureaus.